Electronic Supplementary Material (ESI) for Journal of Materials Chemistry C.

Layered $HgPSe_3$ single crystal: a new candidate for X-ray to visible light photodetectors

Liping Liao[a,], Evgeniya Kovalska[b], Vlastimil Mazanek[a], Lukáš Valdman[a], Lukáš Dekanovsky[a], Bing Wu[a], David Sedmidubský[a], Jan Luxa[a], Štěpán Huber[a], Artur P. Herman[c], Robert Kudrawiec[c], Zdenek Sofer[a,*]*

[a] Department of Inorganic Chemistry, University of Chemistry and Technology, Technicka 5, 166 28, Prague, Czech Republic

[b] College of Engineering Mathematics and Physical Sciences, University of Exeter, EX4 4QF, Exeter, United Kingdom

[c] Department of Semiconductor Materials Engineering, Wrocław University of Science and Technology, Wyspiańskiego 27, Wrocław 50-370, Poland

*Corresponding authors, E-mail addresses: Zdenek Sofer, soferz@vscht.cz, liaol@vscht.cz

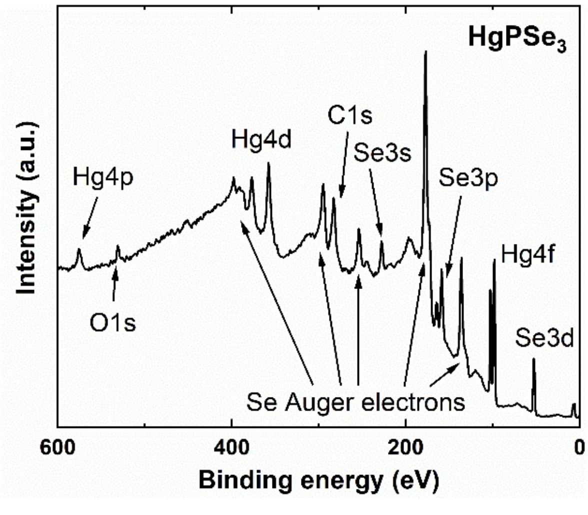

Figure S1. XPS full survey spectrum of $HgPSe_3$ crystal.

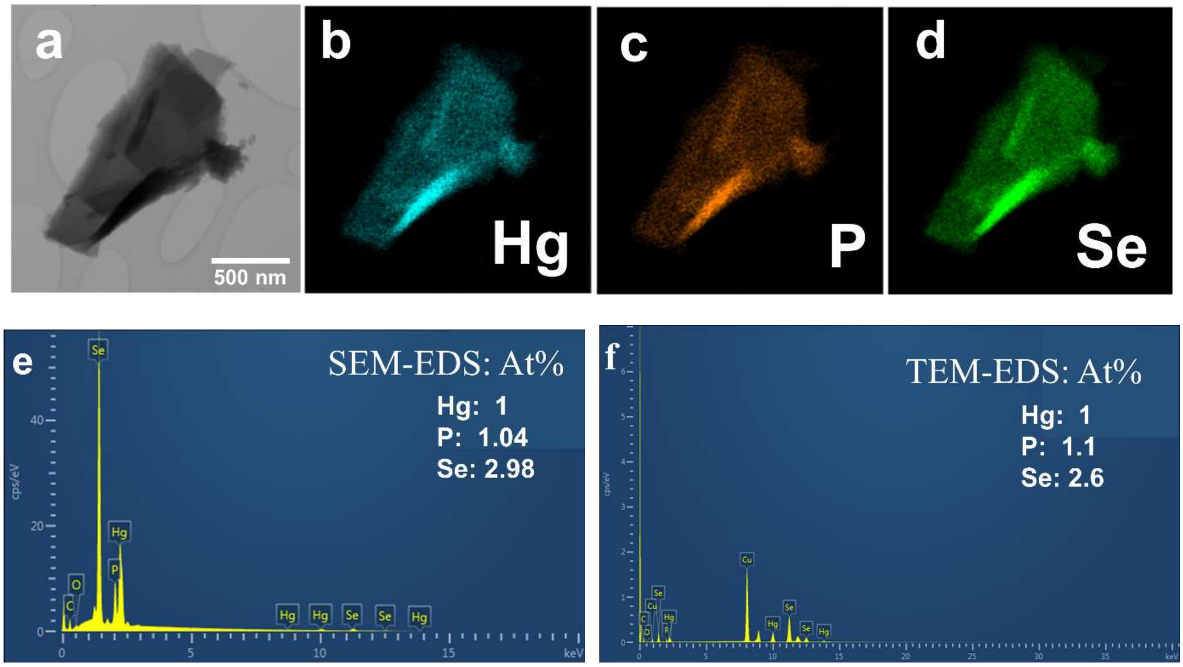

Figure S2. Characterization of $HgPSe_3$ crystal. (a) Low-magnification TEM image. (b,c,d) Corresponding TEM-EDS elemental mapping: Hg, P, Se; and (e,f) elemental spectra.

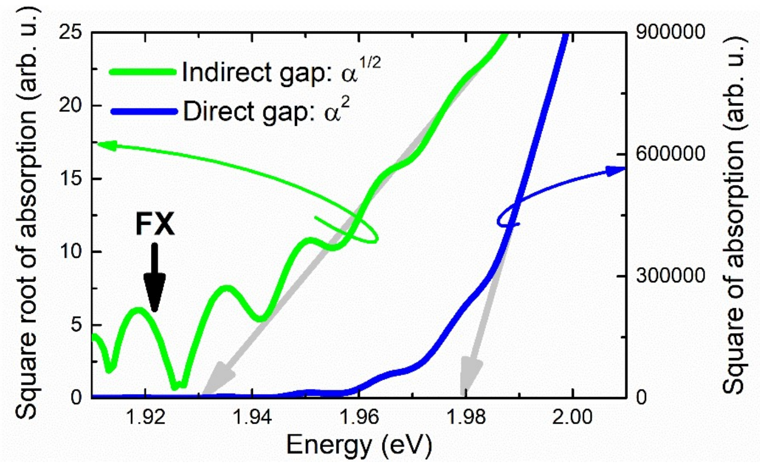

Figure S3. An exemplary analysis of room temperature optical absorption spectrum: square root of absorption (green line) typical for the indirect absorption and square of absorption (blue line) typical for the direct absorption.

Table S1. The calculated stoichiometric ratio from SEM-EDS and TEM-EDS.

	Hg	**P**	**Se**	**Hg : P : Se**
SEM-EDS	2.13	2.03	6.36	1 : 1.04 : 2.98
TEM-EDS	6.1	7.0	15.9	1 : 1.1 : 2.6

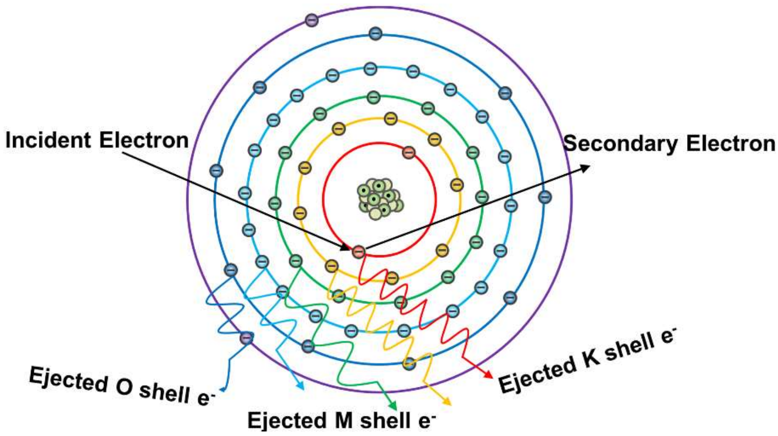

Figure S4. Mechanism investigation of conversion X-ray photon to electrical signals conversion by $HgPSe_3$ crystal.

Table S2. Binding energies of electrons on the different shells of Hg, P, Se atoms.

Z	Element	Electron binding energy (eV)													
		K	L1	L2	L3	M1	M2	M3	M4	M5	N1	N2	N3	N4	N5
		1s	2s	$2p_{1/2}$	$2p_{3/2}$	3s	$3p_{1/2}$	$3p_{3/2}$	$3d_{3/2}$	$3d_{5/2}$	4s	$4p_{1/2}$	$4p_{3/2}$	$4d_{3/2}$	$4d_{5/2}$
80	Hg	83102	14839	14209	12284	3562	3279	2847	2385	2295	803	681.0	576.9	379.0	359.3
15	P	2144	187.7	130.33	135.60	170.0	166.5	160.7	55.5	54.6					
34	Se	12658	1652	54.80	1434.6	230.10	159.50	159.50	55.50	55.40	22.95				

Table S3. Comparison of thermal noise and shot noise under different light wavelengths.

Light wavelength	Responsivity [A/W]	$i_{thermal}$ [A/Hz]^(0.5)	i_{shot} [A/Hz]^(0.5)
Red (650 nm)	4.38×10^{-1}	1.95×10^{-10}	1.13×10^{-14}
Green (530 nm)	2.81×10^{-1}	2.43×10^{-10}	1.15×10^{-14}
Blue (460 nm)	1.96×10^{-1}	2.90×10^{-10}	1.11×10^{-14}
UV (375 nm)	1.77×10^{-1}	3.09×10^{-10}	1.13×10^{-14}

(*bias voltage: 10 V; light power intensity: 0.12732 mW cm^{-2})

The parameters used in calculating noise have been elaborated as follows.

The thermal noise:

$i_{thermal} = (4 \times K_B \times T/\mathrm{R})^{\wedge(0.5)}$

The shot noise:

$i_{shot} = (2 \times e \times I_{off})^{\wedge(0.5)}$

where K_B is Boltzmann constant ($1.38064852 \times 10^{-23}$ m^2 kg s^{-2} K^{-1}); T is the room temperature (300 k); R is the responsivity; e is the elementary charge.

So, we could assume that thermal noise plays a major role in the total noise, since the thermal noise is four orders of magnitude more than shot noise. Thermal noise generated by the thermal agitation of electrons in a semiconductor could explain the limited sensitivity of our photodetector.

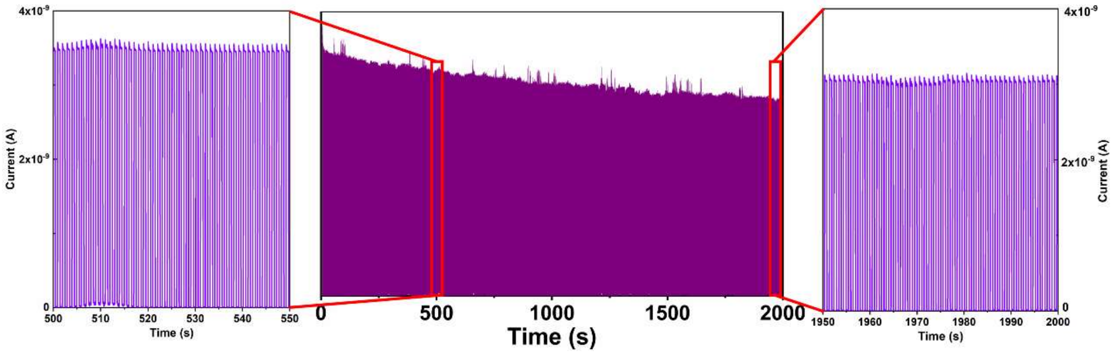

Figure S5. Long-term photo-response curves of $HgPSe_3$ device.

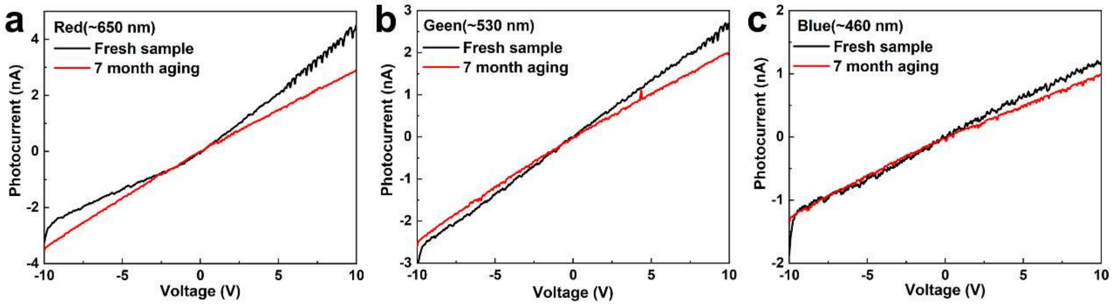

Figure S6. I-V curves of an $HgPSe_3$ device under different light sources: comparison of fresh and 7 months aging conditions in the ambient atmosphere.

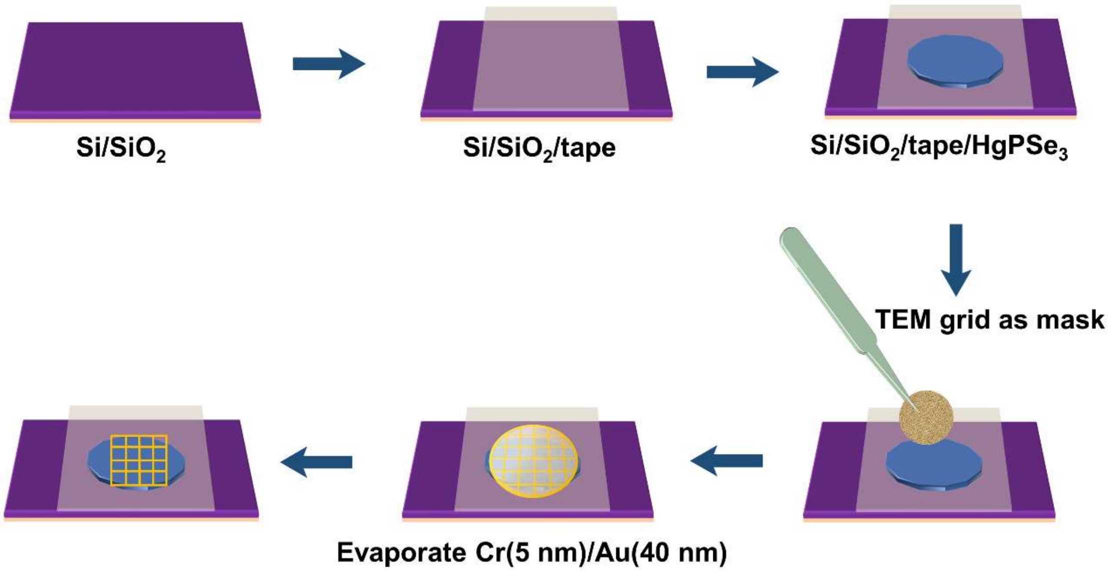

Figure S7. Schematic diagram of $HgPSe_3$ device fabrication process.